Gallium and indium nanomaterials for environmental protection

Marinela Panayotova[1,*], *Vladko* Panayotov[2], and *Tetiana* Oliinyk[3]

[1]University of Mining and Geology, 1 "Boyan Kamenov" Str., Sofia, 1700, Bulgaria
[2]Bulgarian Academy of Sciences, 1 "15 Noemvri" Str., Sofia, 1040, Bulgaria
[3]Kryvyi Rih National University, 11 Vitalii Matusevych Str., Kryvyi Rih, 50027, Ukraine

Abstract. Recent advances in preparation and use of gallium and indium nanoparticles and nanocomposites are briefly presented. The following applications of the obtained materials are outlined: (i) Preparation of sensors for measuring in air of gaseous pollutants (carbon monoxide, nitrogen dioxide, hydrogen sulfide, ammonia, ozone, hydrogen), vapours of volatile organic compounds (methanol, ethanol, butanol, acetone, liquefied petroleum gas), and humidity, including the basics of the sensing mechanism; (ii) removal of water pollutants by photocatalysis and/or adsorption. Finally, conclusions are drawn about the potential of gallium and indium nanoparticles and nanocomposites and the further studies needed to achieve the implementation of these materials in the real life.

1 Introduction

Gallium (Ga) and indium (In) are minor metals applied in advanced technologies needed for the society sustainable development and for our everyday comfortable life. Gallium arsenide is mainly used to manufacture integrated circuits (ICs) and optoelectronic devices. Gallium nitride (GaN) is used to produce optoelectronic devices. For example, Ga consumption in ICs was 68% of the total Ga used in 2018 in the USA, optoelectronic devices accounted for 30%, the left to 100 % was used in research and development, medicine, etc. [1]. In Europe the electric and electronic equipment (EEE) sector is the main user of Ga - 95 % of the element usage [2].

Indium is used mainly as indium tin oxide (ITO). ITO thin-film coatings are employed mainly for electrical conductive purposes in different flat-panel displays. Other In uses are alloys and solders, compounds, semiconductors and electrical components, and research [3]. In the European Union the EEE sector is the major user of In (81 %) [2]. Application of In and Ga in the advanced renewable energy technologies (solar cells, electrodes for hydrogen (H_2) production via water splitting, etc.) and the environment protection activities (pollutants sensing, monitoring and removal) is gaining increased interest recently.

Expected problems with Ga and In supply led to these metals classification in 2017 as critical for Europe materials [4] and as critical for the USA - in 2018 [5]. Materials with high supply risk and above the average economic importance compared to the other raw materials are classified as critical. Increasing the comprehensive use of those metals can be pointed out as one of the measures aimed at mitigation of their expected shortage. Application of nanosized particles (NPs) and nanomaterials, with significant surface area at low mass, may be a step in this direction. In addition, nanomaterials' characteristics are size-dependant and their properties can be tuned by changing the particles size and morphology. The exceptional properties of NPs and nanomaterials attracted the attention of scientists and a tremendous amount of work has been carried out in the area of synthesis, characterization and use of those materials in industry, medicine and the environment protection.

Work on the synthesis and use of Ga and In based nanomaterials has been increasing in the recent years. Present paper is devoted to the latest studies in this area. Applications (still niche) of Ga and In NPs and nanomaterials for green energy production and the environment protection are reviewed. An attempt is made to present examples covering the diversity of these applications.

2 Sensors for air pollution

Carbon monoxide (CO) results in elevated concentrations in the environment mainly from anthropogenic activity (industry, transport). Inhaling CO can cause headache, dizziness, fatigue, to affect hearth and damage the nervous system. Higher exposure to CO can cause sleepiness, hallucinations, convulsions, loss of consignees while extremely high exposure leads to coma and death. The Occupational Safety and Health Administration Agency (OSHA) of the USA limits the long-term workplace exposure levels, i.e. the permissible exposure limit (PEL) for human, to 50 ppm. The USA National Institute for Occupational Safety and Health (NIOSH) places airborne exposure limit (REL) at 35 ppm which should not be exceeded at any time and 200 ppm not to be exceeded during any 15-minute period [6].

Nitrogen dioxide (NO_2) is produced by automotive vehicles and industry. It is one of the main factors of the

* Corresponding author: marichim@mgu.bg

formation of acid rain and the hole in the ozone layer. NO_2 possesses hazardous effects on human health. OSHA places the PEL at 5 ppm averaged over an 8-hour work shift, while the NIOSH's REL is 1 ppm averaged over 10 hour shift [6]. The World Health Organization reports that short-term exposure at concentrations exceeding 200 $\mu g/m^3$ (106 ppb) NO_2 leads to significant negative health effects to humans [7]. That is why advance is needed in portable gas sensors which could detect NO_2 at ppb level.

Hydrogen sulfide (H_2S) causes nausea, dizziness and high exposure may cause a pulmonary edema. OSHA places the PEL at 20 ppm, while the NIOSH's REL is 10 ppm, which should not to be exceeded during any 10-minute period [6].

Ozone (O_3) can affect humans and animals even when it is in very low concentrations, causing irritation of respiratory system, headache and burning eyes. Continuing exposure to O_3 increases the risk of respiratory diseases, and at high concentrations O_3 has lethal effects. OSHA places the PEL at 0.1 ppm, and the NIOSH's REL is 0.1 ppm [6].

Ammonia (NH_3) is an irritant gas and its influence increases with its concentration. Higher exposures to NH_3 may cause pulmonary edema, while repeated exposure – asthma-like allergy and lung damage. Its increased concentrations in the atmosphere are due to anthropogenic sources, mainly use of NH_3 and its derivatives as agricultural fertilizers, but also - industry. OSHA places the PEL at 50 ppm, while the NIOSH's REL is 25 ppm, and 35 ppm have not to be exceeded during any 15-minute period [6].

Hydrogen (H_2) is flammable and explosive at the volume concentration higher than 4% in air [8]. It is expected to be extensively used in production of green and renewable energy in the future, so it is of high importance to develop a low-cost and effective H_2 sensor for practical use at working areas to provide early leakage and explosion warning.

Gas sensors have become a very important part of air quality monitoring, safe industry, etc. Development of commercial gas sensors based on semiconductor metal oxides (SMOs) has acquired a lot of attention, due to their low cost, and the simpe use. Due to their ability to change the conductivity when they are contacting with the gas molecules, SMOs, among them indium oxide (In_2O_3) and gallium oxide (Ga_2O_3), are widely used in the electrical detection of polluting gases. The gas measurements are based on the change in the conductivity of the sensor due to the surface chemical reaction between the sensor's surface and the reducing or oxidizing measured gases. It is commonly acknowledged that the sensing of the n-type semiconductors is controlled by the resistance changing that is brought about by the adsorption and desorption of gas molecules on the surface of the sensor [9-14] as described below. When the sensor is exposed in air, the O_2 molecules from the air capture electrons from the semiconductor's conduction band (CB). Chemisorbed oxygen species (O_2^- O^-, and O^{2-} – depending on the temperature) are generated on the surface of sensing material – equations (1-4). Electron-depleted near-surface region in the semiconductor is formed with the resulting electrical resistance of the sensor, denoted as R_a. When oxidative gas, like NO_2, is introduced into the air, it captures electrons from the CB of the semiconductor, and it also combines with the adsorbed oxygen species, equations (5-6). This results in a decrease in electron concentration in the near-surface region, thereby the depletion layer and the sensing material resistance (denoted as R_g) increase. The ratio R_g/R_a is defined as the sensor's response. The sensors are recovered by placing in air, where species, like NO_2^-, adsorbed on the sensor surface are desorbed - equation (7).

$$O_{2(gas)} \rightarrow O_{2(ads)} \quad (1)$$

$$O_{2(ads)} + e^- \rightarrow O_{2(ads)}^- \quad (< 150\ ^oC) \quad (2)$$

$$O_{2(ads)}^- + e^- \rightarrow 2O_{(ads)}^- \quad (150 - 400\ ^oC) \quad (3)$$

$$O_{(ads)}^- + e^- \rightarrow O_{(ads)}^{2-} \quad (> 400\ ^oC) \quad (4)$$

$$NO_{2(gas)} + e^- \rightarrow NO_{2(ads)}^- \quad (5)$$

$$NO_{2(gas)} + O_{2(ads)}^- + 2e^- \rightarrow NO_{2(ads)}^- + 2O_{(ads)}^- \quad (6)$$

$$NO_{2(ads)}^- + O_{(ads)}^- + e^- \rightarrow NO_{(gas)} + O_{2(ads)}^- \quad (7)$$

When the sensor is exposed to reducing gas (for example, CO, methanol or ethanol vapour, etc.) a redox reaction occurs between the adsorbed oxygen species and the molecules of the measured gas-equations (8-10).

$$2CO + O_{(ads)}^- \rightarrow CO_2 + e^- \quad (8)$$

$$CH_3OH + 3O_{(ads)}^- \rightarrow CO_2 + 2H_2O_{(g)} + 3e^- \quad (9)$$

$$C_2H_5OH + 6O_{(ads)}^- \rightarrow 2CO_2 + 3H_2O_{(g)} + 6e^- \quad (10)$$

Electrons are released and returned to the semiconductor's CB. This leads to the decrease of sensor's resistance. In this case the sensor's response is defined as the ratio R_a/R_g.

Two main directions are used to influence the interaction between the SMOs surface and target gas and thus to improve the gas sensing properties: (i) Application of nanomaterials, including decoration with metal NPs, since the performance of SMOs based sensors strongly depends on grain size, specific surface area and morphology of the sensing material. These properties can be tuned by carefully choosing the synthesis and processing conditions; (i) Doping – that improves the gas sensors characteristics by changing the energy-band structure and morphology, increasing the surface to volume ratio and as a result – creating more centers for gas interaction on the SMOs' surface. In addition, the dopant can act as catalyst that promotes the adsorption and surface reactions and hence improves the sensor performance by increasing the sensor response, reducing response and recovery time, reducing the operating temperature, and increasing selectivity.

2.1 Gallium NPs based sensors

Zinc oxide (ZnO) is one of the earliest and most often used gas-sensing materials. The similarities between ZnO and GaN gave raise to the interest in studying the gas sensing properties of GaN nanostructures. A hybrid structure,

based on GaN, namely Au@rGO/GaN nanorods (NRs), has been developed [15]. The Au@rGO/GaN NRs showed good response to 20 ppm CO that was attributed to interband transition in UV light and the localized surface plasmonic resonance in visible region. According to the authors [15], the Schottky junction (a specific property of reduced graphene oxide - rGO) contributed to the separation and transport of the photogenerated carriers. The Au NPs introduced electronic and chemical changes in the hybrid structure for improving photodetector's response towards CO.

Gallium doped ZnO (GZO) nanocrystalline films have been synthesized by radio frequency magnetron sputtering and their gas sensing properties with respect to H_2S were investigated [16]. Doping lead to enhanced sensing characteristics of the fabricated gas sensors and increased stability with respect to oxidation. Studies confirmed that among the doped films, GZO containing 3 wt. % Ga exhibited the highest sensitivity for H_2S at an operating temperature of 300 °C. The enhanced sensitivity of GZO for H_2S is attributed to the combined effect of excess oxygen vacancies due to Ga^{3+} substitution and the large adsorption energy of Ga that favours chemisorption.

Sensors based on core-shell Pt@ZnO NPs doped with 1 and 2 mol % Ga have been prepared and utilized in acetone[a] and NO_2 sensing [17]. It is found that detection limit to acetone and NO_2 of the 1 mol % Ga doped Pt@ZnO based sensor was 10 ppb and 20 ppb correspondingly.

Composite material Ga_2O_3/Al_2O_3 has been synthesized by a two-step method including hydrothermal and calcining processes [18]. It is shown that Ga_2O_3 nanorods were dispersed on the surface of mesoporous 2D Al_2O_3 nanosheets. The Ga_2O_3/Al_2O_3 composite showed relatively good NO_x (i.e. NO_2 + NO) gas sensing performance. Its response to 100 ppm NO_x at room temperature was 58.2%, being 6.5 times higher than that of pure Ga_2O_3 and remained unchanged for 30 days. The composite material showed ~6 times higher sensitivity to NO_x (100 ppm) compared to HN_3 (100 ppm), ~16 times higher sensitivity compared to CO (1000 ppm), and ~16 times higher sensitivity compared to ethanol (1000 ppm) at room temperature.

2.2 Indium NPs based sensors

Sensors based on In_2O_3 or applying In_2O_3 as doping or decorating materials in other SMOs have been extensively developed and studied recently – for both inorganic and organic gases. Below are presented some examples.

Detection of low CO concentrations at room temperature still poses some challenges. Use of nanomaterials and nanocomposites are among the often considered possible solutions to the problem. Sensing of CO (1–5 ppm) at room temperature by using Zn doped In_2O_3 nanowire (NW) transistors was shown [19]. The doped In_2O_3 NW sensor exhibited enhanced response compared to pure In_2O_3 NW. Relatively good selectivity to CO gas was achieved at comparison with NO and NO_2 (6 and 2 times higher sensor's response correspondingly). The improved response of the prepared sensor at room temperature is assigned to the created defects and to the change in conductivity of the nanowire as a result of Zn-doping.

Two materials ($In_4Sn_3O_{12}$ NPs and $In_4Sn_3O_{12}$–TeO_2 composite NPs) have been synthesized by hydrothermal route and their gas-sensing properties toward CO were examined at different concentrations (5–100 ppm) of CO in the temperature range of 100–300 °C [9]. The $In_4Sn_3O_{12}$–TeO_2 composite NPs sensor showed better sensing performance with response of 10.21, the response and recovery time of 19.73 s and of 217.5 s correspondingly for 100 ppm CO at 200 °C. The improved properties of the sensor are attributed mainly to the enhanced modulation of the potential barrier formed at the $In_4Sn_3O_{12}$–TeO_2 interface, the stronger O_2 adsorption on the TeO_2 (a p-type semiconductor), and the creation of favoured adsorption sites. The $In_4Sn_3O_{12}$–TeO_2 based NPs sensor showed selectivity (2-3 times higher response) to CO (100 ppm) over NH_3 (100 ppm), HCHO (100 ppm) and H_2 (1000 ppm).

A gas sensor based on cobalt (Co)-doped In_2O_3 NPs / molybdenum disulfide (MoS_2) nanoflowers nanocomposite has been prepared and tested with respect to CO (1, 5, 10, 50, 100, 500, 1000, 1500, and 2000 ppm) at room temperature [20]. The Co-In_2O_3/MoS_2 sensor achieved high sensitivity, fast response/recovery speed (response/recovery times = 39 s / 81 s), excellent repeatability and longterm stability (over one month). The high-performance CO sensing was attributed to the Co^{2+} ion doping and heterojunctions created at interface between Co-In_2O_3 and MoS_2.

Zinc oxide is widely used as a basis for preparing gas sensors. However, for the majority of ZnO based gas sensors, the lowest detectable concentration of CO is usually several hundreds of ppm. These values are higher compared to OSHA PEL. In order to improve the sensitivity of ZnO gas sensors for CO monitoring, In-doped ZnO semiconductor NPs (IZO NPs) materials were prepared by a sol-gel technique [21]. The materials were used to fabricate sensors that showed enhanced sensitivity to CO (50 ppm at 300 °C), compared to sensor based on pure ZnO, especially the sensors containing 1 at. % and 2 at. % In.

SMOs are promising choices for hydrogen sensors. Flame spray pyrolysis was used to synthesize palladium oxide (PdO_x)-doped In_2O_3 NPs (5 - 20 nm) [22]. From thus obtained NPs sensing films were prepared by spin coating and tested for their ability to measure H_2 at temperatures ranging from 150 to 350 °C in dry air. The studies revealed that the H_2-sensing characteristics of In_2O_3 NPs were considerably improved by PdO_x doping, especially at the optimal Pd content of 0.50 wt. %. The sensing film showed a response of 3526 towards 10000 ppm H_2 at 250 °C (the optimal working temperature), at response time of 2 s and recovery time of 180 s. Moreover, PdO_x doped In_2O_3 sensing films possessed good stability

[a] Here and further in the text where a comparison is made with volatile organic compounds their vapors are meant.

and high H_2 selectivity against different gases, such as H_2S, NO_2, C_2H_4O, C_2H_4, C_2H_5OH and C_2H_2. The sensing mechanism is described by interaction of H_2 molecules with the preadsorbed oxygen species – reactions (11 – 13):

$$H_{2(g)} \rightarrow 2H_{(ads)} \quad (11)$$

$$2H_{(ads)} + O_{(ads)}^{-} \rightarrow H_2O_{(g)} + e^{-} \quad (12)$$

$$2H_{(ads)} + O_{(ads)}^{2-} \rightarrow H_2O_{(g)} + 2e^{-} \quad (13)$$

The processes produce H_2O and release the trapped electrons back to In_2O_3 CB, thus decreasing the sensor's resistance. The improved gas-sensing behavior is assigned to the effect of the formed p-n heterojunction of PdO_x-In_2O_3 and the presence of PdO_x crystallites which catalyze the dissociation of the H_2 molecules adsorbed on the material's surface.

The number of studies on NO_2 sensor development is expanding recently. Sensors based on In_2O_3 NPs are promising in the NO_2 determination.

Packed In_2O_3 nanospheres have been synthesized via one-step solvothermal method followed by annealing [23]. The NO_2 gas sensing properties of thus prepared nanospheres were studied. The sensor showed response of 217.5 to 500 ppb NO_2, good stability and repeatability at the optimum operating temperature of 120 °C, with a detection limit lower than 10 ppb.

Doping and decoration of In_2O_3 nanomaterials with different metals is considered as a useful route for decreasing the sensors' operational temperature and the measured concentration ranges.

NO_2 sensors able to be used in ppb range of the pollutant concentrations were fabricated on the basis of Ag NPs decorated on hierarchical In_2O_3 nanospheres (Ag / In_2O) [10]. Fast response and recovery times of 30 s and 27 s correspondingly and detection limit of 0.5 ppb of NO_2 were found by using the synthesized Ag / In_2O sensor. Maximum sensitivity of 58 and 25.5 were achieved for 10 ppb of NO_2 at 120 °C for Ag / In_2O_3 sensor and primary In_2O_3 sensor correspondingly. Approximately 2.4-fold increase of NO_2 responses of the Ag / In_2O_3 sensor is observed compared to the response of primary In_2O_3 nanospheres to the concentrations ranging from 1 to 50 ppb of NO_2. Very good selectivity towards NO_2 was found – responses to 50 ppb of NO_2 were 110.2 and 265.6, respectively for primary In_2O_3 sensor and Ag / In_2O_3 sensor, compared to responses in the range of 1.3 - 2.8 and 1.6 - 4.8, respectively to 50 ppm of each of C_2H_5OH, CH_3OH, C_6H_6, $C_6H_5CH_3$, HCHO and CH_3COCH_3. The great performance of the Ag / In_2O_3 sensor is assigned to the hierarchical architecture of In_2O_3 nanospheres, the spill-over effect of metal Ag and the catalytic activity of Ag.

Ordered zirconium (Zr)-doped In_2O_3 (having Zr content of 0.5 wt%) with the pore sizes around 3 nm and undoped In_2O_3 nanostructures were synthesized via nanocasting and tested for their NO_2 gas sensing properties in the concentration range of 20-1000 ppm and the temperature range of 50-140 °C [24]. The Zr-doped In_2O_3 based sensor showed response of 169 toward 1 ppm NO_2 at the operating temperature of 75 °C, 3 times higher than that based on undoped In_2O_3. A detection limit of 20 ppb was achieved by the Zr-doped In_2O_3. At 75 °C the Zr-doped In_2O_3 sensor exhibited much higher response towards 500 ppb NO_2 against other gases (10 ppm H_2S, 10 ppm NH_3, 100 ppm ethanol, 100 ppm acetone, 1 ppm SO_2, 1 ppm Cl_2, 500 ppb O_3). The enhanced properties of the Zr-doped In_2O_3 based sensor are ascribed to the ability of Zr-doping to increase the amount of chemically adsorbed oxygen and limit crystallites' size. In addition, the increased electrons' concentration of Zr-doped In_2O_3 makes its resistance very low thus facilitating its employment in portable devices.

Li and co-authors [11] proposed NO_2 sensors based on highly ordered In_2O_3, prepared by nanocasting method using mesoporous silica as template and decorated with Au NPs. The optimal sensor, based on 0.5 wt. % Au-loaded In_2O_3, possessed a response of 472 (7.1 times higher than the response of pure In_2O_3 based sensor) and a detection limit of 10 ppb at operating temperature of 65 °C. The selectivity of the sensor towards various gases, such as NH_3 – 100 ppm, Cl_2 – 10 ppm, CH_4 – 10 ppm, H_2S – 1 ppm, CO – 10 ppm, SO_2 – 10 ppm, and O_3 – 500 ppb, was studied. The response to NO_2 was ~ 100 fold higher compared to the selectivity to other gases, except of O_3, where it was ~ 10 fold higher. The excellent sensing properties of the Au NPs decorated In_2O_3 based sensor were mainly attributed to the ordered mesoporous structure and the catalytic activity of Au.

Ag-doped hollow urchin-like In_2O_3 hierarchical nanostructures were developed by solvothermal route followed by thermal treatment. They have been tested for NO_2 detection in the concentration range of 0.05 – 1.5 ppm NO_2 and the operation temperature range of 50 – 150 °C [25]. Best results were obtained for the sensor with 1.0 mol % Ag - with response of 190 to the target gas (1 ppm NO_2) at operating temperature of 62 °C. The sensor response increased almost linearly with increasing the concentration of NO_2 from 50 to 1000 ppb. The sensors based on Ag-doped In_2O_3 hierarchical nanostructures showed relatively fast response time (~5 min) and recovery time (~8 min). The sensor based on 1.0 mol % Ag doped In_2O_3 showed higher response to 1 ppm NO_2 (over 200 fold) in the presence of various gases (SO_2, Cl_2, CH_4, CO, C_2H_4, each one – 10 ppm and C_2H_5OH - 100 ppm) at 62 °C. The enhanced NO_2 sensing performance of Ag-doped In_2O_3 is attributed to its hierarchical structure and the catalytic activity of Ag NPs.

A metal-organic frameworks-derived In_2O_3 hollow microtubes / molybdenum disulfide NPs (In_2O_3/MoS_2) nanocomposite film sensor has been prepared using a layer-by-layer self-assembly method and its sensitivity towards 0.1–100 ppm NO_2 was studied at temperature of 25 °C [26]. It is found that the In_2O_3/MoS_2 composite sensor exhibited a response value of 371.9 toward 100 ppm NO_2, which is higher than the response of individual In_2O_3 sensor (of ~ 110). The sensor possesses a good linearity in the range 0.1 – 100 ppm NO_2 and reversibility. The response value of the In_2O_3/MoS_2 film sensor to 10 ppm NO_2 is much higher than towards the same concentrations of CH_2O, NH_3, C_2H_5OH, $(CH_3)_2CO$, C_6H_6, and H_2S, indicating high selectivity towards NO_2. The In_2O_3/MoS_2 nanocomposite-based sensor showed good

repeatability and stability upon exposure to 5, 10 and 100 ppm NO_2. The enhanced NO_2-sensing properties were assigned to the synergistic effects of In_2O_3 hollow microtubes and MoS_2 NPs.

Recently, improving the sensors characteristics by irradiation with UV light has been proposed. Walnut-like In_2O_3 nanostructures have been directly grown on the interdigited electrode substrate by using a hydrothermal approach, followed by a thermal treatment [13]. The synthesized walnut-like In_2O_3 nanostructures have been used to fabricate a photoelectric gas sensor that was studied in the range of 0.1–50 ppm NO_2. A linear dependence of sensitivity on the NO_2 concentration was observed and the sensor showed sensitivity of 219 towards 50 ppm NO_2 when subjected to irradiation (1.2 mW/cm^2) of UV light (λ=365 nm). The sensor possessed response of ~ 32 to 5 ppm NO_2 in the presence of other gases (50 ppm SO_2, 100 ppm CH_4, and 100 ppm CO) at room temperature. The sensitivity to the other gases was < 5 showing selectivity toward NO_2. The high performance of the walnut-like In_2O_3 was assigned to its high specific surface area, the enhanced interface force between the gas sensor substrate and the active material and effective participation of the photo-generated electrons.

Ozone has to be monitored in industrial applications (requiring high O_3 concentrations) and for the human and the environment protection, where low concentrations have to be measured. However, the majority of the commercial sensors are properly working only in one of the concentration ranges – low (ppb) or high (ppm). Indium oxide NPs can be used to solve the problem. A cheap portable photostimulated ozone sensor, based on In_2O_3 NPs, has been developed that was able to measure O_3 in the concentration range over four orders of magnitude at room temperature by changing the diameter of the In_2O_3 NPs [27]. It is based on the findings that the 7-nm In_2O_3 NPs can detect O_3 concentration between 10 ppb and 10 ppm, while the 12-nm NPs are suitable for O_3 detection between 10 and 200 ppm. By combining the two types of NPs, O_3 in the concentration range of 10 ppb – 200 ppm can be measured. The sensors' response to 12 ppb O_3 remained stable even in the presence of 1200 ppb CO, 100 ppm CO_2, or 100 ppb NO_2. However, increasing the NO_2 concentration up to 200 ppb lead to slightly higher response than that to pure 12 ppb O_3, while the response to 40 ppb O_3 was unchanged. The sensing signal was reproducible and hysteresis was not observed in measurements conducted for 35 hours. A small influence of the low humidity on the sensor response was observed. Sensor signals were found to be reproducible in a high-humidity gas environment and thus they can be accounted for. By sealing the sensor chamber with a porous hydrophobic membrane, which prevented the passage of liquid water, submerged measurements were carried out [28].

An organized monitoring of NH_3 concentrations is essential for decreasing the hazard for human health and plants. Regardless of this, the measurement of atmospheric NH_3 in urban areas has been usually unconsidered, since its average concentrations are generally low (in the 20–30 ppb range). A low-cost sensor based on a mixture of single-walled carbon nanotubes (SWCNT) bundle layers with indium-tin oxide (ITO) NPs was prepared on plastic substrate [29]. The sensor exhibited high sensitivity to NH_3 (detection limit of 13 ppb) when used at room temperature. It displayed short recovery time and high selectivity in the presence of acetone and ethanol. The functionalized SWCNT exhibit a resistivity decrease when are exposed to water concentrations representative for ambient air (in the ppm range), revealing the possibility to differentiate the impact of interfering water vapour signal in the NH_3 measurement.

Methanol (CH_3OH) vapour causes headache, irritation of the eyes and mucous membranes. The repeated exposure to CH_3OH vapour may lead to metabolic acidosis, serious visual impairment, difficult to breathe. The OSHA PEL is 200 ppm, while the NIOSH REL is 200 ppm, and 250 ppm have not to be exceeded during any 15-minute period [6].

Pure ethanol (C_2H_5OH) irritates the skin and eyes. OSHA placed the PEL at 1000 ppm and the NIOSH's REL is also 1000 ppm [6]. Recently some studies have paid attention to the health risks related to inhalation of C_2H_5OH vapour [30].

Acetone ($(CH_3)_2CO$) vapour is irritating; exposure to its high concentrations affects eyes, nose and throat. The acetone PEL is 1000 ppm, the REL is 250 ppm [6].

The liquefied petroleum gas (LPG) vapour, when present in high concentrations in the air, can cause suffocation with symptoms of headache, dizziness, weakness, nausea, vomiting. The LPG PEL is 1000 ppm averaged over an 8-hour work shift, while the REL is 1000 ppm averaged over 10 hour shift [6].

Exposure to n-butanol vapours can cause headache, dizziness, nausea, vomiting. OSHA's PEL is 100 ppm averaged over an 8-hour work shift, while the REL placed by NIOSH is 50 ppm which should not be exceeded at any time [6].

In order to protect humans and the environment, sensors are needed that are able to detect the above-mentioned vapours.

Anand and co-authors synthesized pure and Ag-doped (1, 3 and 5 % Ag) In_2O_3 NPs by the co-precipitation method and studied their sensing properties towards CH_3OH, C_2H_5OH, $(CH_3)_2CO$ and LPG at different operating temperatures [31]. Best results were obtained with 3% Ag-doped NPs whose maximum response (R_a/R_g) was ~30 towards C_2H_5OH at the operating temperature of 300 °C, ~15.5 towards $(CH_3)_2CO$ at 350 °C, ~17 towards LPG at 400 °C and ~12 – towards CH_3OH at 300 °C – at the concentration of 50 ppm of each tested gas. The response time for In_2O_3 – 3% Ag sensor was between 6 and 32 s while for undoped In_2O_3 sensor – between 10 and 40 s, depending on the measured concentration. The improved sensing performance of 3% Ag-doped NPs based sensor is assigned to (i) the large number of oxygen vacancies leading to increased amount of O_2 adsorbed on the sensor surface as compared to pure In_2O_3 sensor, and (ii) the catalytic effect of Ag – Ag improves the sensor response by the formation of activated species of the chemisorbed analyte, which are

then spilled onto the surface of In_2O_3. That results in fast reaction between the analyte molecule and oxygen.

Liu and co-authors further decreased the optimum measuring temperature and the concentration range (from 1 ppm to 50 ppm) by demonstrating C_2H_5OH gas sensor based on indium oxide / molybdenum disulfide (In_2O_3/MoS_2) nanocomposite prepared via hydrothermal route [12]. The reported sensor response at 260 ºC for In_2O_3/ MoS_2 composite was ~36, while for pristine In_2O_3 it was ~ 14 at 280 ºC. The responses of the two sensors show almost constant value to 50 ppm of C_2H_5OH at 260 ºC over 50 days, demonstrating the high stability of these sensors. The In_2O_3/MoS_2 sensor showed selectivity to C_2H_5OH (150 ppm) in presence of C_6H_6 (250 ppm), $(CH_3)_2CO$ (350 ppm), NH_3 (450 ppm), and H_2O (5500 ppm). The improved characteristics of In_2O_3/ MoS_2 nanocomposite sensor, compared to pristine In_2O_3 sensor are assigned to the large specific surface and good electrical properties of MoS_2, as well as to the synergistic effect between In_2O_3 and MoS_2. It is suggested that the MoS_2 nanosheets provide a platform for attaching In_2O_3 NPs, hampering their interparticle aggregation and providing more active sites for the adsorption of C_2H_5OH molecules. It is concluded that the fabricated nanostructure favors molecular adsorption, gas diffusion and mass transport, thus improving the gas sensing performance.

Shruthi and co-authors prepared sensor based on Y_2O_3-In_2O_3 nanocomposites [14] and conducted gas sensing studies under room temperature. The Y_2O_3-In_2O_3 sensor responses of ~923 and 3.722 were found towards 200 ppm and 1 ppm CH_3OH correspondingly. The response and recovery times of Y_2O_3-In_2O_3 were 13 and 18 s respectively and the sensor showed stability over 30 days. The response and Y_2O_3-In_2O_3 gas sensor towards 200 ppm CH_3OH in presence of other gases (ethanol, n-butanol, acetyl acetone, ammonia, isopropanol, xylene, toluene, 2-methoxyethanol, acetone, and cyclohexane – each one 200 ppm) at room temperature was between 4.5 and 20 times higher compared to the response to the other gases thus proving the sensor's high selectivity. The enhanced properties of Y_2O_3-In_2O_3 sensor were explained by the formation of a n-n hetero junction between Y_2O_3 and In_2O_3 and the appearance of built-in potential.

Porous In_2O_3 NPs (20 - 50 nm) were prepared using a solvothermal method and studied as gas-sensing material for n-butanol – 50 ppm [32]. At 140 °C the sensor showed responses of 5.5, 10.3, 20.5, 32.4, 54.7, 97.3, and 241 for n-butanol concentrations of 5, 10, 15, 20, 30, 50, and 100 ppm, correspondingly. The sensor exposed to 50 ppm of other gases (ethanol, acetone, formaldehyde, benzene, xylene, methanol, ammonia, and n-butanol) exhibited good selectivity to n-butanol vapor. The good response of In_2O_3 NPs was assigned to their large specific surface area and porous structure that can provide more reactive sites and allow successful transfer of gases.

In some cases In_2O_3 is used as one of the components of nanocomposite applied as a sensing material. Humidity detection and measurement is one of the important parameters in the environment monitoring. Graphene oxide/Nafion/indium oxide (GO/Nafion/In_2O_3) nanocomposite - based humidity sensor has been made-up and tested under a wide relative humidity range (RH = 11–97 %) at 25 °C [33]. The GO/Nafion/In_2O_3 film humidity sensor exhibited high sensitivity (especially at RH > 80%), low hysteresis, good stability and repeatability. The sensor work is based on the increase in the capacitance with the increase in the RH, since the amount of water molecules physisorbed on the sensor surface increases as RH increases. The water molecules, possessing a dipole moment, can increase the capacitance of the nanocomposite.

Doping of other materials used for sensors with In compounds improves the performance of these materials. Crystalline ZnO nanorods were modified by In_2O_3 NPs using PVP as a morphology control agent via sol-gel and the hydrolysis method and the obtained material was used to prepare sensor for n-butanol vapor [34]. Tests showed that the In_2O_3/ZnO sensor response was 104.3 towards the n-butanol concentration of 100 ppm at 370 °C. This was 3.5 and 5.3 times higher than the response of the pure ZnO and In_2O_3 sensor, correspondingly. The response and recovery times of the In_2O_3/ZnO sensor were 6 s and 9 s at the gas concentration of 4 ppm. The response of the In_2O_3/ZnO sensor containing 3.3 mol % of In was 6.1 at n-butanol concentration of 1 ppm, showing good detection. The In_2O_3/ZnO sensor exhibited high selectivity to n-butanol (100 ppm) in the presence of ethanol, methanol, acetone, and ethyl acetate (each one 100 ppm). The enhanced sensing performance was ascribed to the 1D single crystalline nature of ZnO nanorods and the heterostructure established between In_2O_3 and ZnO nanorods.

3 Water pollutants removal

The scientific work has shown that the photocatalytic degradation of toxic organic pollutants is one of the most efficient methods for surface water purification. Ga and In NPs and nanocomposites are gaining their place in this area. The photochemical pollutant removal can result from direct or indirect interactions, or from the both types of reactions – Fig. 1. In the direct reaction pathway (Fig. 1a) the photogenerated holes (or electrons) directly oxidize (or reduce) pollutants that are adsorbed on the photocatalyst surface. In the indirect path (Fig. 1b) the excited electrons move to the surface of photocatalyst and react with O_2 to generate superoxide radical anions ($\bullet O_2^-$). At the same time, the corresponding holes move to the exterior of the photocatalyst and oxidize the water molecules or hydroxyl groups, present on its surface to produce hydroxyl radicals (•OH). Thus formed reactive radical species are able to decompose and mineralize pollutants into CO_2, H_2O and other inorganic species [35]. The light utilization efficiency, cost-performance ratio, and secondary toxicity are the major anxieties in the photocatalytic pollutants' removal.

3.1 Gallium NPs based materials

Titanium dioxide (TiO_2) NPs in anatase form are often used as photocatalyts. Anatase NPs doping with Ga by

applying sol-gel method is reported [36]. The NPs obtained (with size of around 15 nm) were used to study the photocatalytic degradation of organic dye solution (Rhodamine B) as a model pollutant under UV irradiation. Nearly 90% degradation efficiency was achieved within 3 hrs of UV irradiation when Ga-doped TiO_2 NPs were used, which is faster than the Rhodamine B degradation by undoped samples. The effect is ascribed to the fact that doping levels were created within the bandgap of TiO_2. These levels act as trapping centers to suppress the recombination of photogenerated electrons and holes. In this way proper utilization of charge carriers is achieved for the generation of strong oxidizing radicals able to degrade the organic dye. Consequently the derived Ga doped TiO_2 NPs can be used for light-assisted oxidation of toxic organic molecules in the surface water for the environment protection.

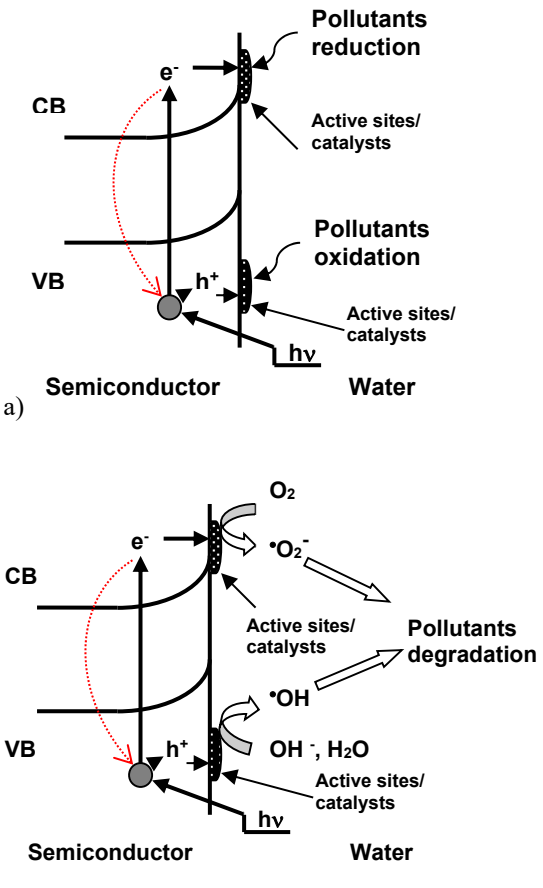

Fig. 1. Schematic representation of electron-hole pairs photo-generation and their participation in pollutants removal: a) direct pollutants oxidation and/or reduction, b) indirect pollutants decomposition. Red dashed arrow – a possibility for recombination of photogenerated electrons and holes.

Fluoride ion (F^-) is mobile under natural conditions and can appear in elevated concentrations in water due to natural leaching of rocks. However, most often its high concentrations are due to anthropogenic activities such as metals' extraction, electroplating, etc. When F^- presents in drinking water in concentrations higher than the recommended, it can cause dental and skeletal fluorosis. With the aim to reduce the F^- concentration in water, different methods have been developed, such as adsorption, ion exchange, precipitation, and membrane processes. Most of them are feasible when applied to point pollution sources. Adsorption can be applied also to polluted water discharged from diffusion pollution sources if the loaded adsorbent can be collected. Use of nanosorbents with magnetic properties is a big step in this direction. Improved selectivity and chemical reactivity are the other desired features of those adsorbents. As contribution in this area Fe_3O_4 NPs were synthesized by coprecipitation of Fe^{2+} and Fe^{3+} under alkaline conditions and their surface was then modified with 3-aminopropyltriethoxysilane (APTES) [37]. The Fe_3O_4/APTES NPs were further modified by grafting Ga tetrakis (4-carboxyphenyl) porphyrin groups at their surface. The batch experiments using thus prepared NPs showed that they can be applied to remove F^- from aqueous solution. Extraction efficiency over 96% was achieved at an initial F^- concentration of 10 mg/L, pH 5.5 and contact time of 30 min. The Fe_3O_4/APTES/Ga nanosorbent was successfully regenerated by using NaOH solution. The recovery of F^- ions from the adsorbent under optimum conditions was 98%. The fluoride removal efficiency by the Fe_3O_4/APTES/Ga nanoadsorbent in 5 adsorption / regeneration cycles was 97.2%, 96.8%, 95.5%, 94.3%, and 87.0% correspondingly, showing the adsorbent stability.

3.2 Indium NPs based materials

In this application mainly indium sulfide (In_2S_3) materials are used, based on their photocatalytic properties. Due to its stability and low-toxicity In_2S_3 (with UV-Vis-NIR – solar-spectrum) can be used as promising photocatalyst and a sensitizer for other semiconductors with photocatalytic properties. The proper separation and transport of photo-induced charge carriers is one of the promising ways for improving the efficiency of In_2S_3-based materials for pollutants' removal. Efforts have been made to decrease the recombination of photogenerated electron-hole pairs by morphology design, doping or producing heterostructured materials. The studies on nanosized In-based materials usage for water pollutants removal are devoted mainly to organic dyes, pharmaceuticals and microorganisms removal.

Gao and co-authors [38] have controlled the morphology of In_2S_3 NPs, thus adjusting the mass-transfer pathway for the photocatalytic removal of pollutants in the liquid-phase system. The tetragonal In_2S_3 NPs with size of 5–20 nm, synthesized by them, showed stable photo-catalytic removal of methyl orange (MO) over the entire solar light spectrum - under UV light (96.2% within 30 min), visible light (95.4% within 3 h) and near-infrared light (67.2% within 3 h). The broad light absorption region of the synthesized NPs is assigned to the presence of a defect band located above the VB of In_2S_3.

Wu and co-authors [39] prepared a porous 3D microsphere-like In_2S_3, stacked by 2D ultrathin nanosheets, which showed 3 times higher photo-degradation efficiency with respect to MO compared to 3D solid microsphere-like In_2S_3. The better photocatalytic

activity was attributed to the relatively higher specific surface area and the presence of more reaction sites, which accelerated the surface separation of photo-induced charges and the inter-facial charge-carrier transfer.

Li and co-authors [40] prepared In_2S_3–TiO_2 nanotube array composites by CV, potentiostatic and pulse electrodeposition. Their studies showed that the pulse prepared In_2S_3–TiO_2 yielded the highest and stable photocurrent response, consequently showing an excellent photocatalytic activity in the degradation of p-nitrophenol. It was considered that the homogeneous, ultra-fine structure of In_2S_3 NPs lead to a high charge separation efficiency resulting in improved photocatalytic activity.

Self-organized TiO_2 nanotubes (NTs) array was decorated with In_2S_3 NPs to obtain (In_2S_3/TiO_2 NTs) hybrid that exhibited strong absorption in the visible light region and enhanced photocurrent density [41]. The In_2S_3/TiO_2 NTs showed higher photocatalytic activity when compared to that of bare TiO_2 NTs in the degradation of herbicide 2,4-dichlorophenoxyacetic acid (2,4-D) under simulated solar light. Approximately 100 % removal of the 2,4-D was achieved for 160-min irradiation by using the optimum In_2S_3/TiO_2 NTs composition. The removal efficiency was 95.1 % after 10 successive cycles. The photocatalyst has shown a good stability and easy recovery that gives grounds for its potential application for the photocatalytic removal of some organic pollutants from water.

Indium sulfide / zinc germanate (In_2S_3/Zn_2GeO_4) composites, with different In_2S_3 concentrations, were prepared via a co-precipitation hydrothermal method [42] and tested for their ability to decompose acetaminophen (APAP). The composite containing 30 mass % In_2S_3 showed the best activity for APAP degradation under visible light, with better performance compared to In_2S_3, nitrogen-doped TiO_2, TiO_2 powder (Degussa P25), and Zn_2GeO_4. The studies revealed that holes and formed superoxide radicals were mainly involved in the photodegradation of APAP.

Hierarchical nanoflower superstructures consisting of In_2S_3 nanosheets grown on a Bi_2S_3 nanoflower backbone (Bi_2S_3/In_2S_3) were prepared by a solvothermal route, rest on different growth rates of the two sulphides [43]. The as-prepared Bi_2S_3/In_2S_3 material exhibited notable visible-light photocatalytic activity and stability in the degradation of 2,4-dichlorophenol. This is assigned to the presence of In_2S_3 nanosheets on the surface of the Bi_2S_3 nanoflowers which lead to increased visible-light response and enhanced photogenerated charge transport and separation steered by the heterojunction.

Hollow β-In_2S_3 NPs with high surface area have been synthesized by means of anion exchange process under a hydrothermal condition without any surfactant or sacrificial agent [44]. Adsorption capacity and photocatalytic activity of the newly prepared material were assessed, using methylene blue (MB) under dark and visible light irradiation. The big adsorption capacity (ca 158 mg/g in 60 min) for MB in the solution, realized in a fast process, was assigned to the high specific surface area (324.6 m^2/g) of the β-In_2S_3 NPs and to the electrostatic interaction between the negatively charged surface of β-In_2S_3 and the MB. After the adsorption reaction, visible light photocatalytic reaction further decreased the concentration of the still existing MB. The removal efficiency for 100 mg/L of MB solution was 73.4% under dark for 60 min (indicating that adsorption plays an essential role for removing MB), and after further visible light irradiation for 180 min increased to 92.2%.

Tetragonal prismatic γ-In_2Se_3 NPs with the (110) facets were synthesized hydrothermally in the presence of ethylenediaminetetraacetic acid (EDTA) that plays a key role in the exposed facets regulation [45]. Studies on the photocatalytic decomposition of tetracycline (TC) by the newly synthesized material showed that the γ-In_2Se_3 NPs prepared with 0.04 M EDTA had the optimal activity ensuring degradation of TC in 120 min with an efficiency of 91.5%.

Gao and co-authors [46] investigated the visible light photocatalytic disinfection of water by using a photocatalyst prepared via joining non-woven carbon nanofibers (CNF) and In_2S_3 nanoflowers to construct three-dimensional hierarchical CNF–In_2S_3 nanostructures with large specific surface area and enhanced light absorption. Approximately 80 % of *Escherichia coli* cells were killed by CNF-In_2S_3 under visible light irradiation owing to the occurrence of oxidative stress. The good activity of the CNF-In_2S_3 photocatalyst was attributed to the enhanced light absorption, large surface area, and efficient charge separation that facilitate production of oxidizing species.

4 Conclusions

In conclusion, it can be said that Ga and In NPs and nanocomposites are materials showing potential for application in environmental protection. Materials based on Ga and In NPs are proposed for sensors for determining inorganic and organic polluting gases. In this application further work is needed in direction of increasing the response and selectivity in the low ranges of the measured concentrations, and of long-time stability of the prepared sensors (since most of the studies cover only 30 days).

In the water pollutants removal application most of the studies have been conducted with organic dye solutions. Consideration of other types of pollutants seems interesting. More data on the pollutants' decomposition products and investigations on the ways for collecting and separating from the water of the already used photocatalysts are needed.

The improvements in all above-mentioned directions can not be achieved without further research on the mechanisms of the proceeding reactions and phenomena and on the impacting factors.

Ending, we can say that Ga and In NPs and nanocomposites are promising materials but still much work is required for their implementation in the real life devices.

References

1. B.W. Jaskula, in *Mineral Commodity Summaries 2019,* ed. by USGS (Reston, Virginia, 2019), p. 62
2. F. Mathieux, F. Ardente, S. Bobba, P. Nuss, G. Blengini, P. Alves-Dias, D. Blagoeva, C. Torres-De-Matos, D. Wittmer, C. Pavel, T. Hamor, H. Saveyn, B. Gawlik, G. Orveillon, D. Huygens, E. Garbarino, E. Tzimas, F. Bouraoui, S. Solar, *Critical raw materials and the circular economy – background report* (Publications Office of the European Union, Luxembourg, 2017), pp. 39-40.
3. C.S. Anderson, in *Mineral Commodity Summaries 2019*, ed. by USGS (Reston, Virginia, 2019), p. 78
4. European Commission, Communication from the Commission to the European Parliament, the Council, the European Economic and Social Committee and the Committee of the Regions on the 2017 list of Critical Raw Materials for the EU. (COM(2017) 490 final, 2017)
5. The U.S. Department of the Interior, Final List of Critical Minerals 2018 (Federal Register 83 (97) 2018)
6. NIOSH Publications, *NIOSH Pocket Guide to Chemical Hazards* (Cincinnati, Ohio, 2007)
7. World Health Organization, *WHO Air Quality Guidelines-Global Update 2005* (Copenhagen, 2006)
8. Right to know, Hazardous Substance Fact Sheet, Hydrogen (2016), https://nj.gov/health/eoh/rtkweb/documents/fs/1010.pdf. Accessed 06 Dec 2019
9. A. Mirzaei, S. Park, G. J. Sun, H. Kheel, C. Lee, CO gas sensing properties of $In_4Sn_3O_{12}$ and TeO_2 composite nanoparticle sensors. J. Hazard. Mater. **305**, 130–138 (2016). doi:10.1016/j.jhazmat.2015.11.044
10. B. Xiao, S. Song, P. Wang, Q. Zhao, M. Chuai, M. Zhang, Promoting effects of Ag on In_2O_3 nanospheres of sub-ppb NO_2 detection. Sensor. Actuat. B-Chem. **241**, 489–497 (2017). doi:10.1016/j.snb.2016.10.107
11. S. Li, M. Cheng, G. Liu, L. Zhao, B. Zhang, Y. Gao, H. Lu, H. Wang, J. Zhao, F. Liu, X. Yan, T. Zhang, G. Lu, High-response and low-temperature nitrogen dioxide gas sensor based on gold-loaded mesoporous indium trioxide. J. Colloid. Interf. Sci. **524**, 368–378 (2018). doi:10.1016/j.jcis.2018.04.033
12. X. Liu, L. Jiang, X. Jiang, X. Tian, Y. Huang, P. Hou, S. Zhang, X. Xu, Design of superior ethanol gas sensor based on indium oxide/molybdenum disulfide nanocomposite via hydrothermal route. Appl. Surf. Sci. **447**, 49–56 (2018). doi:10.1016/j.apsusc. 2018.03.116
13. H. Ma, Y. Lu, X. Yuan, Y. Li, C. Li, M. Yin, X. Fan, Room temperature photoelectric NO_2 gas sensor based on direct growth of walnut-like In_2O_3 nanostructures. J. Alloy. Compd. **782**, 1121–1126 (2019). doi:10.1016/j.jallcom.2018.12.180
14. J. Shruthi, N. Jayababu, P. Ghosal, M.V.R. Reddy, Ultrasensitive sensor based on Y_2O_3-In_2O_3 nanocomposites for the detection of methanol at room temperature. Ceram. Int. **45**, 21497–21504 (2019). doi:10.1016/j.ceramint. 2019.07.141
15. M. Reddeppa, S.B. Mitta, T. Chandrakalavathi, B.G. Park, G. Murali, R. Jeyalakshmi, S.G. Kim, S.H. Park, M.D. Kim, Solution-processed Au@rGO/GaN nanorods hybrid-structure for self-powered UV, visible photodetector and CO gas sensors. Curr. Appl. Phys. **19**, 938–945 (2019). doi:10.1016/j.cap.2019.05.008
16. K.G. Girija, K. Somasundaram, A.K. Debnath, A. Topkar, R. Vats, Enhanced H_2S sensing properties of Gallium doped ZnO nanocrystalline films as investigated by DC conductivity and impedance spectroscopy. Mater. Chem. Phys. **214**, 297–305 (2018). doi:10.1016/j.matchemphys.2018.04.104
17. Y. Gong, X. Wu, X. Zhou X. Li, N. Han, Y. Chen, High acetone sensitive and reversible P- to N-type switching NO2 sensing properties of Pt@Ga-ZnO core-shell nanoparticles. Sensor. Actuat. B-Chem. **289**, 114–123 (2019). doi:10.1016/j.snb.2019.03.085
18. J. Wang, S. Jiang, H. Liu, S. Wang, Q. Pan, Y. Yin, G. Zhang, P- type gas-sensing behavior of Ga_2O_3/Al_2O_3nanocomposite with high sensitivity to NO_xat room temperature. J. Alloy. Compd. **814** (2020). doi:10.1016/j.jallcom.2019.152284
19. N. Singh, C. Yan, P. S. Lee, Room temperature CO gas sensing using Zn-doped In_2O_3 single nanowire field effect transistors. Sensor. Actuat. B-Chem. **150**, 19–24 (2010). doi:10.1016/j.snb.2010.07.051
20. D. Zhang, J. Wu, Y. Cao, Cobalt-doped indium oxide/molybdenum disulfide ternary nanocomposite toward carbon monoxide gas sensing. J. Alloy. Compd. **777**, 443–453 (2019). doi:10.1016/j.jallcom.2018.10.365
21. R. Dhahri, M. Hjiri, L.E. Mir, H. Alamri, A. Bonavita, D. Iannazzo, S.G. Leonardi, G. Neri, CO sensing characteristics of In-doped ZnO semiconductor nanoparticles. J. Sci. Adv. Mater. Devices **2**, 34–40 (2017). doi:10.1016/j.jsamd.2017.01.003
22. K. Inyawilert, A. Wisitsoraat, C. Liewhiran, A. Tuantranont, S. Phanichphant, H_2 gas sensor based on PdO_x-doped In_2O_3 nanoparticles synthesized by flame spray pyrolysis. Appl. Surf. Sci. **475**, 191–203 (2019). doi:10.1016/j.apsusc.2018.12.274
23. B. Xiao, Q. Zhao, D. Wang, G. Ma, M. Zhang, Facile synthesis of nanoparticle packed In_2O_3 nanospheres for highly sensitive NO_2 sensing. New J. Chem. **41**, 8530–8535 (2017). doi:10.1039/C7NJ00647K
24. Q. Yang, Y. Wang, J. Liu, Y. Gao, P. Sun, Z. Jie, T. Zhang, Y. Wang, G. Lu, Enhanced sensing response towards NO_2 based on ordered mesoporous Zr-doped In_2O_3 with low operating temperature. Sensor. Actuat. B-Chem. **241**, 806–813 (2017). doi:10.1016/j.snb.2016.09.145
25. M. Ding, N. Xie, C. Wang, X. Kou, H. Zhang, L. Guo, Y. Sun, X. Chuai, Y. Gao, F. Liu, P. Sun, G. Lu, Enhanced NO_2 gas sensing properties by Ag-doped

hollow urchin-like In_2O_3 hierarchical nanostructures. Sensor. Actuat. B-Chem. **252**, 418–427 (2017). doi:10.1016/j.snb.2017.06.016

26. Z. Yang, D. Zhang, H. Chen, MOF-derived indium oxide hollow microtubes/MoS_2 nanoparticles for NO_2 gas sensing. Sensor. Actuat. B-Chem. **300** (2019). doi:10.1016/j.snb.2019.127037
27. C.Y. Wang, R.W. Becker, T. Passow, W. Pletschen, K. Köhler, V. Cimalla, O. Ambacher, Photon stimulated sensor based on indium oxide nanoparticles I: Wide-concentration-range ozone monitoring in air. Sensor. Actuat. B-Chem. **152**, 235–240 (2011). doi:10.1016/j.snb.2010.12.014
28. C.Y. Wang, S. Bagchi, M. Bitterling, R.W. Becker, K. Köhler, V. Cimalla, O. Ambacher, C. Chaumette, Photon stimulated ozone sensor based on indium oxide nanoparticles II: Ozone monitoring in humidity and water environments. Sensor. Actuat. B-Chem. **164**, 37–42 (2012). doi:10.1016/j.snb.2012.01.058
29. F. Rigoni, G. Drera, S. Pagliara, A. Goldoni, L. Sangaletti, High sensitivity, moisture selective, ammonia gas sensors based on single-walled carbon nanotubes functionalized with indium tin oxide nanoparticles. Carbon **80**, 356–363 (2014). doi:10.1016/j.carbon.2014.08.074
30. R.R. MacLean, G.W. Valentine, P.I. Jatlow, M. Sofuoglu, Inhalation of alcohol vapor: measurement and implications. Alcohol. Clin. Exp. Res. **41**, 238–250 (2017). doi:10.1111/acer.13291
31. K. Anand, J. Kaur, R.C. Singh, R. Thangaraj, Preparation and characterization of Ag-doped In_2O_3 nanoparticles gas sensor. Chem. Phys. Lett. **682**, 140–146 (2017). doi:10.1016/j.cplett.2017.06.008
32. J. Wang, Z. Zheng, D. An, X. Tong, Q. Zhou, Highly selective n-butanol gas sensor based on porous In_2O_3 nanoparticles prepared by solvothermal treatment. Mat. Sci. Semicon. Proc. **83**, 139–143 (2018). doi:10.1016/j.mssp.2018.04.014
33. D. Zhang, M.Wang, Z. Yang, Facile fabrication of graphene oxide/Nafion/indium oxide for humidity sensing with highly sensitive capacitance response. Sensor. Actuat. B-Chem. **292**, 187–195 (2019). doi:10.1016/j.snb.2019.04.133
34. F. Liu, G. Huang, X. Wang, X. Xie, G. Xu, G. Lu, X. He, J. Tian, H. Cui, High response and selectivity of single crystalline ZnO nanorods modified by In_2O_3 nanoparticles for n-butanol gas sensing. Sensor. Actuat. B - Chem. **277**, 144–151 (2018). doi:10.1016/j.snb.2018.08.144
35. J. Zhang, H. Wang, X. Yuan, G. Zeng, W. Tu, S. Wang, Tailored indium sulfide-based materials for solar-energy conversion and utilization. J. Photoch. Photobio. C **38**, 1–26 (2019). doi:10.1016/j.jphotochemrev.2018.11.001
36. A.N. Banerjee, S.W. Joo, B.K. Min, Photocatalytic degradation of organic dye by sol-gel-derived gallium-doped anatase titanium oxide nanoparticles for environmental remediation. J. Nanomater. (2012). doi:10.1155/2012/201492
37. B. Asgari, J. Bowen, Gallium (III)-Metalloporphyrin Grafted Magnetite Nanoparticles for Fluoride Removal from Aqueous Solutions. Nat. Prod. Chem. Res. **5**, 282 (2017). doi:10.4172/2329-6836.1000282
38. W. Gao, W. Liu, Y. Leng, X. Wang, X. Wang, B. Hu, D. Yu, Y. Sang, H. Liu, In_2S_3 nanomaterial as a broadband spectrum photocatalyst to display significant activity. Appl. Catal. B - Environ. **176–177**, 83–90 (2015). doi:10.1016/j.apcatb.2015.03.048
39. R. Wu, Y. Xu, R. Xu, Y. Huang, B. Zhang, Ultrathin-nanosheet-based 3D hierarchical porous In_2S_3 microspheres: chemical transformation synthesis, characterization, and enhanced photocatalytic and photoelectrochemical property. J. Mater. Chem. A. **3**, 1930–1934 (2015). doi:10.1039/C4TA05729E
40. Y. Li, S. Luo, Z. Wei, D. Meng, M. Ding, C. Liu, Electrodeposition technique-dependent photoelectro-chemical and photocatalytic properties of an In_2S_3/TiO_2 nanotube array. Phys. Chem. Chem. Phys. **16**, 4361–4368 (2014). doi:10.1039/C3CP54675F
41. Z. Zhang, Y. Tang, C. Liu, L. Wan, Fabrication of In_2S_3 nanoparticle decorated TiO_2 nanotube arrays by successive ionic layer adsorption and reaction technique and their photocatalytic application. J. Nanosci. Nanotechnol. **14**, 4170–4177 (2014). doi:10.1166/jnn.2014.8232
42. T. Yan, T. Wu, Y. Zhang, M. Sun, X. Wang, Q. Wei, B. Du, Fabrication of In_2S_3/Zn_2GeO_4 composite photocatalyst for degradation of acetaminophen under visible light. J. Colloid. Interface. Sci. **506**, 197–206 (2017). doi:10.1016/j.jcis.2017.06.079
43. Y. Chen, G. Tian, Q. Guo, R. Li, T. Han, H. Fu, One-step synthesis of a hierarchical Bi_2S_3 nanoflower/In_2S_3 nanosheet composite with efficient visible-light photocatalytic activity. Cryst. Eng. Comm. **17**, 8720–8727 (2015). doi:10.1039/C5CE01747E
44. H. Li, Z. Yuan, C. Bittencourt, W. Li, M. Chen, W. Li, R. Snyders, Anion exchange synthesis of hollow β-In_2S_3 nanoparticles: Adsorption and visible light photocatalytic performances. J. Environ. Chem. Eng. **7** (2019). doi:10.1016/j.jece.2019.102910
45. X. Wei, H. Feng, L. Li, J. Gong, K. Jiang, S. Xu, P. K. Chu, Synthesis of tetragonal prismatic γ-In_2Se_3 nanostructures with predominantly {110} facets and photocatalytic degradation of tetracycline. Appl. Catal. B - Environ. **260** (2020). doi:10.1016/j.apcatb.2019.118218
46. P. Gao, A.R. Li, M.H. Tai, Z.Y. Liu, D.D. Sun, A hierarchical nanostructured carbon nanofiber-In_2S_3 photocatalyst with high photodegradation and disinfection abilities under visible light. Chem. Asian. J. **9**, 1663–1670 (2014). doi:10.1002/asia.201400057